# AN ABSTRACT OF THE THESIS OF

Sarah L. Philo for the degree of Master of Science in Materials Science presented on September 15, 2009.
Title: Effect of Ambient Environment on the Fracture and Fatigue Properties of Zr-Based Bulk Metallic Glasses

Abstract approved:

_____

Jamie J. Kruzic

The effect of ambient environment on the fatigue behavior of two Zr-Ti-Cu-Ni-Be bulk metallic glasses (BMGs) is examined in the present study. The first metallic glass, $Zr_{44}Ti_{11}Ni_{10}Cu_{10}Be_{25}$, was tested to establish the presence of an environmental effect in the fatigue growth curve measured in ambient air. Fatigue growth curves produced from $Zr_{44}Ti_{11}Ni_{10}Cu_{10}Be_{25}$ in ambient environment were shown to exhibit a plateau where the fatigue growth rate was independent of stress intensity range near $10^{-9}$ m/cycle, which are typically characteristic of aggressive environment, affecting crack growth. Experiments performed in inert atmosphere (dry $N_2$) demonstrated a higher threshold stress intensity ($\Delta K_{TH}$), near-threshold crack growth rates decreased significantly, and no stress intensity independent plateau was measured. It was therefore confirmed that the fatigue behavior of $Zr_{44}Ti_{11}Ni_{10}Cu_{10}Be_{25}$ is significantly affected by aggressive ambient air environment. Both oxidation and hydrogen embrittlement processes are discussed as possible causes for the observed environmental effect. An initial study of the fatigue properties of the second metallic glass, $Zr_{58.5}Cu_{15.6}Ni_{12.8}Al_{10.3}Nb_{2.8}$, was performed. A fatigue growth curve was

produced in ambient atmosphere and a plateau in the fatigue growth curve near $2.5 \times 10^{-8}$ m/cycle was measured. In the plateau produced by $Zr_{58.5}Cu_{15.6}Ni_{12.8}Al_{10.3}Nb_{2.8}$ the growth rate was independent of stress intensity, like in the fatigue curve measured from $Zr_{44}Ti_{11}Ni_{10}Cu_{10}Be_{25}$ under similar conditions. It is speculated that $Zr_{58.5}Cu_{15.6}Ni_{12.8}Al_{10.3}Nb_{2.8}$ is susceptible to an environmental species more diffusive in $Zr_{58.5}Cu_{15.6}Ni_{12.8}Al_{10.3}Nb_{2.8}$ than that found to affect $Zr_{44}Ti_{11}Ni_{10}Cu_{10}Be_{25}$, because the characteristic plateau occurs at a higher growth rate. The plane strain fracture toughness ($K_C$) was also measured for $Zr_{58.5}Cu_{15.6}Ni_{12.8}Al_{10.3}Nb_{2.8}$ and found to equal ~26 MPa√m. However, crack branching was discovered to have occurred during each $K_C$ measurement, making the accuracy of the measurements difficult to ascertain.

# Effect of Ambient Environment on the Fracture and Fatigue Properties of Zr-Based Bulk Metallic Glasses

by
Sarah L. Philo

A THESIS

submitted to

Oregon State University

in partial fulfillment of
the requirements for the
degree of

Master of Science

Presented September 15, 2009
Commencement June 2010

Master of Science thesis of Sarah L. Philo presented on September 15, 2009.

APPROVED:

_____

Major Professor, representing Materials Science

_____

Director of the Materials Science Program

_____

Dean of the Graduate School

I understand that my thesis will become part of the permanent collection of Oregon State University libraries. My signature below authorizes release of my thesis to any reader upon request.

_____

Sarah L. Philo, Author

# ACKNOWLEDGEMENTS

I would like to sincerely thank Dr. Jamie Kruzic for his infinite patience and wisdom throughout the experimentation and writing processes. He has been an invaluable source of knowledge, guidance, and motivation.

I would also like to thank:

- Minalben Shah, Sarah Gallops, and Rawley Greene for all of their help with almost every aspect of my research,
- Dr. Ralf Bush and Dr. Isabella Gallino for their input and insight,
- Maximilien Launey for stress relieving my samples and for valuable advice,
- Joshua Hogg and Travis Burns for machining my samples,
- Dr. William Warnes for unwittingly donating his vacuum pump,
- Christopher Shelton and Dr. Brady Gibbons for their help with the XRD and for generously donating Dr. Warnes' vacuum pump,
- Eric Patterson, Christopher Dandenau and Seunghwa Kwon for help with the XRD,
- and Teresa Sawyer for her help with the SEM.

I would like to thank everyone in the Materials Science Department at Oregon State, Michael, and my friends and family for their countless contributions.

# CONTRIBUTION OF AUTHORS

Dr. Ralf Bush, Dr. Isabella Gallino, and Hao Lu formed and cast the Vit 106a samples, and will be involved in writing the final submission of the manuscript contained in Chapter 3.

# TABLE OF CONTENTS

# LIST OF FIGURES

## LIST OF FIGURES (Continued)

Figure Page

# LIST OF TABLES

# I. Introduction

Metallic glasses, glassy metals, or amorphous metals are solids formed by rapidly quenching molten metals or metal alloys. An almost instant quenching process, usually on the order of hundreds of degrees Kelvin per second or more, inhibits the large scale atomic organization that allows crystal formation in traditional metals.

The first metallic glass was discovered in 1960 by the immediate quenching of a molten alloy comprised of gold and tin [1]. Due to the high rate of cooling necessary to prevent formation of crystal structures, technologies evolved to mass produce thin metallic glass ribbons and sheets, but it was not until 1988 that metallic glasses could be formed in bulk [2]. Bulk metallic glasses (BMGs) are alloys that are generally found to crystallize approximately ten or more times slower than their thinner metallic glass counterparts, enabling them to be cast into larger forms (thickness >1mm) while maintaining an amorphous structure [3]. While metallic glasses have been studied for nearly fifty years, new bulk metallic glass forming alloys are still being discovered.

Metallic glasses provide several mechanical advantages over crystalline metals; they achieve near-ideal strength in both tension and compression, can be precisely cast or otherwise formed, and demonstrate high elastic strain and low damping [4]. There are also disadvantages; the most prominent drawback is that metallic glasses typically fail catastrophically due to the combination of strain softening behavior and unstable shear band formation. Each alloy has a distinct set of material properties, and it is necessary to determine the characteristics of alloys before they are considered for specific mechanical applications.

The fatigue behavior of two metallic glasses is considered; $Zr_{44}Ti_{11}Ni_{10}Cu_{10}Be_{25}$, known as Vitreloy 1b or Vit 1b, and $Zr_{58.5}Cu_{15.6}Ni_{12.8}Al_{10.3}Nb_{2.8}$, commonly referred to as Vitreloy 106a or Vit 106a. The Vitreloy family of BMGs contains some of the best glass forming alloys, such as $Zr_{41.25}Ti_{13.75}Ni_{10}Cu_{12.5}Be_{22.5}$, or Vitreloy 1™, patented by Liquidmetal© Technologies and used in several commercial applications [5]. Vit 1b and Vit 106a have both demonstrated excellent glass forming ability, and Vit 106a is touted as one of the best known beryllium-free metallic glass forming alloys, with a critical cooling rate as low as 1.75 K/s [6, 7].

This document contains two manuscripts that are to be submitted for publication in scientific journals. Both documents analyze the fatigue properties of metallic glasses, and assess the effects of aggressive environment on fatigue behavior. The first manuscript, “Fatigue crack growth behavior of a Zr-Ti-Cu-Ni-Be bulk metallic glass: Role of ambient air environment,” verifies the effect of aggressive environment on the fatigue properties of $Zr_{44}Ti_{11}Ni_{10}Cu_{10}Be_{25}$ measured in ambient air, and examines the susceptibility of zirconium-based metallic glasses to oxide and hydrogen embrittlement mechanisms. The second manuscript, “Fracture and fatigue behavior of a $Zr_{58.5}Cu_{15.6}Ni_{12.8}Al_{10.3}Nb_{2.8}$ bulk metallic glass forming alloy,” is an initial analysis of the fracture and fatigue behavior of $Zr_{58.5}Cu_{15.6}Ni_{12.8}Al_{10.3}Nb_{2.8}$.

# II. Bulk Metallic Glasses

## *2.1 Relevant Properties*

Unlike crystalline metals, metallic glasses have no highly-structured, evenly spaced lattice with specific and periodic atomic arrangement. Instead, amorphous metals maintain an atomic arrangement similar to that found in its liquid state, with atoms densely packed together without specific placement or spacing. The high level of organization detailed for crystalline metals is referred to as long-range order (LRO), and describes a predictable configuration of atoms throughout the material. Metallic glasses demonstrate no long-range order; however, arbitrary portions of a given volume of material often exhibit some repeated atomic arrangement, termed short- or medium-range order, depending on the relative size of the volume of ordered atoms. A given volume demonstrating short range order (SRO) is typically less than 0.5 nm in radius, and medium range order (MRO) can be found up to a radius of about 1 nm [4]. SRO and MRO are important because they enable the material to achieve near-ideal atomic spacing [4].

When an amorphous material is dense-packed, atoms in the material are arranged such that any given atom is as close to the atoms surrounding it as is physically possible. Any structural deviation from dense-packing will result in the creation of free space in the material, called free volume. Therefore, a material with no free volume ($v_f$) is dense-packed. The solidification and deformation of BMGs will create free volume, and annealing will reduce $v_f$. The presence of free volume allows

for atomic diffusion within the material, and increasing free volume eases plastic deformation, increases fracture toughness ($K_C$), and decreases fatigue life [5].

Because BMGs are amorphous, deformation cannot occur as the motion of defects through the material, as it does in crystalline metals. Instead, BMGs generally demonstrate large scale deformation behavior characterized by the creation of shear bands and subsequent motion along shear banded planes. Shear band propagation is the primary mode of fracture in both tension and compression for metallic glasses, and often causes catastrophic failure in amorphous metals. Shear bands are thin (~10 nm initially) layers of material that flow under high stresses, and form at stress concentrations found in regions with increased amounts of free volume [8, 9]. In compression, elastic recovery often leads to the termination of one or several shear bands; multiple shear bands can form and terminate before one propagates through the whole of the material. In tension, typically only one shear band will expand to failure. Shear band formation and expansion is an almost-instantaneous process, causing BMGs to fail in tension without any apparent prior deformation. The process is so rapid because metallic glasses shear soften—that is, their viscosity decreases dramatically when plastically deformed [9].

### *2.2 Fracture and Fatigue of Metallic Glasses*

Fracture in metallic glasses, as previously described, occurs by the formation and propagation of shear bands through the material. Critical stress intensity, or fracture toughness ($K_C$), is a measurement of a material's resistance to fracture. It is a

function of the length of the crack in the material (a) and the applied stress at fracture of the material ($\sigma_y$), and can be modeled as follows:

$$K_C = Y\sigma_y\sqrt{\pi a} \qquad (1)$$

where Y is a unitless function dependent on sample geometry. Fracture occurs when the stress intensity is greater than or equal to the critical stress intensity. Table 1 lists typical $K_C$ values for the BMG alloys discussed in this study.

**Table 1: Reported fracture toughness ($K_C$) values for relevant bulk metallic glasses.**

| Composition | Alloy Name | $K_C$ Value (MPa√m) |
|---|---|---|
| $Zr_{41.25}Ti_{13.75}Ni_{10}Cu_{12.5}Be_{22.5}$ | Vitreloy 1™ | 44 ± 24 [5, 10, 11] |
| $Zr_{44}Ti_{11}Ni_{10}Cu_{10}Be_{25}$ | Vitreloy 1b | 34 [12] |
| $Zr_{58.5}Cu_{15.6}Ni_{12.8}Al_{10.3}Nb_{2.8}$ | Vitreloy 106 a | ~26 |

While the properties of BMG deformation can be observed on a large scale, the exact mechanism behind deformation on an atomic scale, like that created by cyclic loading, or fatigue testing, is still largely undetermined. The general mechanism of deformation in metallic glasses that can be found in the literature is based on theories of atomic movement. Atomic rearrangement in the form of the motion of atomic clusters likely causes both internal stresses and an increase in free volume thereby allowing for further motion of other atomic clusters and therefore permanent deformation of the material (See Figure 1) [13-16].

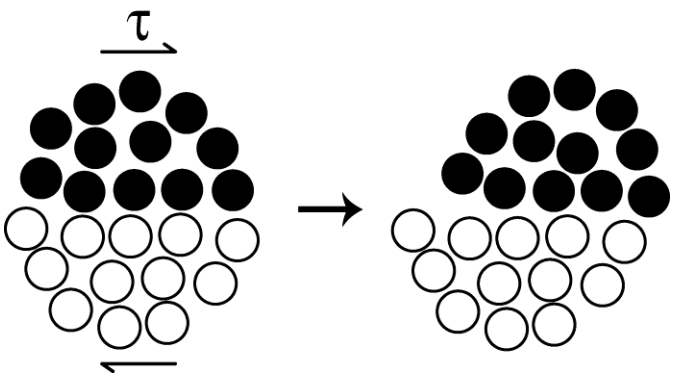


**Figure 1: Motion of atomic clusters in an amorphous material: an atomic rotation of the darker top cluster of atoms relative to the lighter cluster at the bottom.**

The specific mechanism of atomic-scale plastic deformation; whether the concentration of internal stress or the increase in free volume induced by the motion of atomic clusters causes (or further creates) increased internal stress concentrations and free volume formation, is more highly debated. Both theories are equally viable: it makes sense that free volume creation will cause stress concentrations around the newly formed volume of empty space, and that unevenly distributed stress concentrations would cause atomic volumes in higher stress areas to move into areas of lower stress, thereby creating free volume. Therefore, the creation and propagation of free volume due to the existence of stress concentrations and/or pre-existing free volume is a probable phenomenon, as is the creation and propagation of stress concentrations due to the existence of free volume and/or pre-existing stress concentrations, and both likely occur in some form.

On a larger scale, fatigue growth curves of BMGs look much like those of crystalline metals, shown in Figure 2, where $da/dN$ is the change in crack length per loading cycle, or crack growth rate, and $\Delta K$ is the stress intensity range. $\Delta K$ is equal to

the difference between the maximum and minimum stress intensities sustained during the loading cycle ($\Delta K = K_{max} - K_{min}$). They typically display a three-region curve:

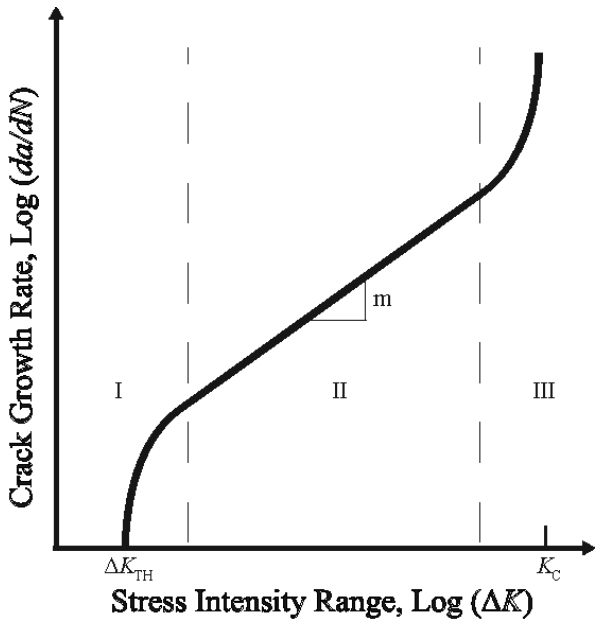


**Figure 2: Characteristic fatigue growth curve for metals.**

Region I contains $\Delta K_{TH}$, the threshold stress intensity. Below this value for $\Delta K$, cracks should not grow, and *da/dN* approaches zero. In Region I the crack growth rate (*da/dN*) is very sensitive to changes in stress intensity [17].

Region II is called the Paris or Mid-Growth-Rate region. Region II can be modeled by the Paris equation [18]:

$$\frac{da}{dN} = c\,\Delta K^{m} \qquad (2)$$

where c and m are material constants. Typical values for m lie between 2 and 4 for most metals, including metallic glasses.

Region III contains $K_C$, where final fracture occurs. In Region III, the crack rapidly accelerates as $K_{max}$ approaches $K_C$. It is here that larger-scale failure mechanisms begin; microvoid coalescence in crystalline metals, or shear band formation in BMGs.

*2.3 Environment-Sensitive Fatigue Curves*

Environmental corrosion can affect fatigue growth curves in three ways, shown in Figure 3, where *da/dN* is the crack growth rate, and $\Delta K$ is the stress intensity range:

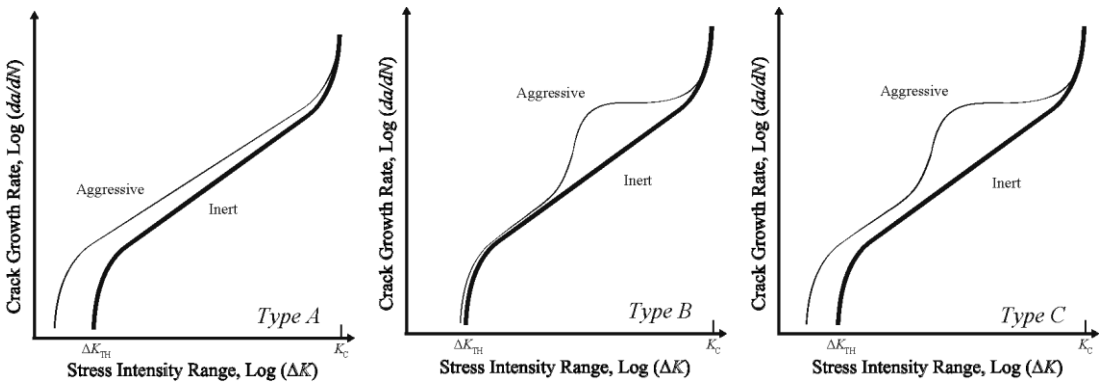


**Figure 3: Types of environmental effect on the fatigue curve of metals.**

Type A demonstrates crack growth that is cycle dependent and time independent [19], and can be mathematically modeled by multiplying the inert fatigue growth rate by an acceleration factor:

$$\left(\frac{da}{dN}\right)_{\text{Aggressive}} = \Phi\left(\frac{da}{dN}\right)_{\text{Inert}} \quad (3)$$

where the increase in crack growth rate ($\Phi$) may be constant, or it may change with $\Delta K$ [17]. $\Delta K_{TH}$ is sensitive to aggressive environment,

fatigue crack acceleration is independent of loading frequency, and a synergistic relationship exists between plastic deformation in the material and the environment [19].

Type B is time dependent and cycle independent [19], and can be modeled by superimposing the environmental crack growth rate over the inert crack growth rate:

$$\left(\frac{da}{dN}\right)_{\text{Aggressive}} = \left(\frac{da}{dN}\right)_{\text{Inert}} + \frac{1}{f}\left(\frac{d\bar{a}}{dt}\right)_{\text{EAC}} \quad (4)$$

where f is the loading frequency, and $(d\bar{a}/dt)_{EAC}$ is the average environmental crack growth rate per loading cycle[17]. This type of fatigue curve is often produced in high strength metals [19]. $K_{TH}$ is not usually sensitive to this type of environmental effect [19].

Type C occurs when a material exhibits both cycle and time dependence [19], and can be modeled as the superposition of type A and B fatigue curves:

$$\left(\frac{da}{dN}\right)_{\text{Aggressive}} = \Phi\left(\frac{da}{dN}\right)_{\text{Inert}} + \frac{1}{f}\left(\frac{d\bar{a}}{dt}\right)_{\text{EAC}} \quad (5)$$

where Φ is the increase in crack growth rate, f is the loading frequency, and $(d\bar{a}/dt)_{EAC}$ is the average environmental crack growth rate per loading cycle [17]. $K_{TH}$ is may or may not be environment sensitive [19].

*2.4 Environment and the Fatigue Behavior of Metallic Glasses*

Oxidation and hydrogen embrittlement are two prominent environmentally assisted cracking (EAC) mechanisms found to affect metals, and zirconium-based BMGs are particularly susceptible to both processes. During cyclic fatigue of metallic glasses, high stress concentrations are induced at the crack tip, causing plastic deformation and increasing the free volume in the plastic zone surrounding the crack tip [12, 20]. Increases in free volume have been shown to decrease corrosion current density and corrosion resistance [21].

During oxidation, an oxide film typically forms along the walls of the crack, allowing environment to access the fresh material at the crack tip exclusively [17]. High stresses at the crack tip rupture the oxide layer, subjecting the surface to further corrosion. The primary oxidation mechanism known to affect fatigue behavior is crack wedging. Crack wedging occurs when a thick layer of oxide forms along the crack walls. The oxide layer wedges the crack tip open during the relaxation phase of the fatigue cycle, causing compression in the material [17]. Most metallic glasses typically form thin, passive amorphous oxide layers with low ionic and electrical conductivity [22]. Zr-based BMGs are potentially vulnerable to crack wedging because exposure to ambient air at room temperature causes rapid preferential oxidation of Zr over other elements, forming a layer of $ZrO_2$ in nanoseconds [23, 24]. Crack wedging diminishes $\Delta K_{apparent}$ at stress intensities near $\Delta K_{TH}$, and is very sensitive to the ratio of $K_{min}/ K_{max}$, known as the R ratio, being more pronounced at lower R ratios [17, 19]. It is postulated by King, *et. al.* that oxide wedging has no effect after the threshold

regime (Region I in Figure 2), and that in the Paris Regime (Region II in Figure 2) an adherent thin oxide layer with low coefficient of diffusion and high fracture strain should help minimize oxygen assisted crack growth [24].

Hydrogen embrittlement of metals may occur in two ways: bond-decohesion, and hydride formation. Bond-decohesion is the most prominent hydrogen embrittlement mechanism; hydrogen absorbs into the material in the plastic zone adjacent to and ahead of the crack tip, weakening the inter-atomic bonds between by lengthening the average distance between bonded atoms [17, 19]. Hydrogen can also form brittle hydrides within the bulk of the material [22]. Metallic glasses that contain any amount of free volume are susceptible to hydrogen embrittlement. Because H atoms are so small, they can freely adsorb into the free volume of metallic glasses [22, 25, 26]. Zr-based alloys have an increased tendency toward H absorption near Zr atoms, and are particularly vulnerable to brittle hydride formation [22, 27]. However, hydride formation has not yet been documented in the fatigue of Zr-Ti-Ni-Cu-Be BMGs [28, 29]. In the case of BMGs specifically, it is also theorized that plastic deformation at the crack tip is impeded by H atoms occupying much of the once available free volume, inducing a loss of plasticity [25, 29]. The specific mechanism for plasticity loss due to free volume saturation is thought to occur by impeding the redistribution of stresses on an atomic level near the crack tip, curbing stress relief [29]. Suh, *et. al.* claim that the effect of hydrogen occupation of free volume is strong enough to negate any plasticity gained from free volume expansion at the crack tip [29].

# III. Manuscript I

## Fatigue Crack Growth Behavior of a Zr-Ti-Cu-Ni-Be Bulk Metallic Glass: Role of Ambient Air Environment

S. L. Philo and J. J. Kruzic[1]

Materials Science, School of Mechanical, Industrial, and Manufacturing Engineering,

Oregon State University, Corvallis, Oregon, 97331, USA

Submitted to

*Scripta Materialia*

[1] Corresponding author. Tel: +1-541-737-7027; fax: +1-541-737-2600.
*E-mail address:* jamie.kruzic@oregonstate.edu (J. J. Kruzic)

**Abstract**

The fatigue crack growth behavior of a $Zr_{44}Ti_{11}Ni_{10}Cu_{10}Be_{25}$ bulk metallic glass (BMG) was measured in an inert dry $N_2$ environment. When compared to results measured in ambient air, the present results showed a higher fatigue threshold and lower crack growth rates in the near threshold region. Such results reveal that there is a significant corrosion fatigue effect in ambient air for this BMG.

## 1. Introduction

Bulk metallic glasses (BMGs) are a relatively new class of engineering materials with unique and unusual properties that make them potential candidates for many structural applications.[30] Favorable properties include near theoretical strengths combined with reasonable fracture toughness, low damping, large elastic strain limits, and the ability to be thermoplastically formed into precision shaped parts with complex geometries [31, 32], all of which are generally distinct from, or superior to, corresponding crystalline metals and alloys. One property which has been perceived as a limitation for BMGs has been low fatigue resistance relative to crystalline metallic materials [33]; however, not all studies to date have been in agreement on this point. For the most studied BMG, $Zr_{41.25}Ti_{13.75}Ni_{10}Cu_{12.5}Be_{22.5}$,[2] the reported $10^7$ cycle fatigue strengths vary by a factor of seven [34, 35], and fatigue thresholds vary by a factor of three[34]. While some of the reported scatter may be explained by different testing configurations [36], this does not account for all the observed variations, for example, those within single studies [5, 34]. Clearly there is a

[2] All compositions are given in terms of atomic percent.

need for more fundamental understanding of fatigue mechanisms and the factors that govern fatigue behavior.

The effect of aggressive environments on the fatigue properties of crystalline metals is a relatively well studied phenomenon; however, there is a dearth of information with regard to environmental effects on amorphous metals. It is interesting to note that many of the features of crystalline metals that may promote interactions with the environment, such as grain boundaries or dislocations, simply do not exist in metallic glasses. Nonetheless, both hydrogen embrittlement and surface oxidation have been reported for various amorphous metals [22, 23, 25, 26, 28, 29, 37-43], either of which could affect fatigue crack growth via traditional crack tip embrittlement, film rupture, or oxide induced closure mechanisms.

Fatigue crack growth data collected in ambient room air for $Zr_{41.2}Ti_{13.8}Cu_{12.5}Ni_{10}Be_{22.5}$ and $Zr_{44}Ti_{11}Ni_{10}Cu_{10}Be_{25}$ bulk metallic glasses (BMGs) found in the literature generally display a plateau in the crack growth curve at around $10^{-9}$ m/cycle where the growth rate is relatively insensitive to the applied stress intensity range [11, 12]. In the fatigue of materials, such behavior generally indicates something other than mechanical loading acts as the rate limiting step in the crack growth process, and that commonly is an interaction with the environment [44, 45]. Accordingly, the purpose of this paper is to determine if corrosion fatigue indeed occurs in Zr-Ti-Cu-Ni-Be BMGs in ambient air by measuring the fatigue crack growth rates of $Zr_{44}Ti_{11}Ni_{10}Cu_{10}Be_{25}$ in dry high purity nitrogen and comparing them to previously reported fatigue crack growth data for testing conducted in room air.

## 2. Experimental Methods

### *2.1. Materials*

Fully amorphous $Zr_{44}Ti_{11}Ni_{10}Cu_{10}Be_{25}$ plates, cast and provided by Liquidmetal© Technologies (Lake Forest, CA), were machined into compact tension C(T) samples (width, $W$ = 20 mm, thickness, $B$ = 3 mm) compliant with the ASTM E647 standard [46]. The surfaces of each sample were then polished to a 0.05μm finish to allow accurate crack length measurements.

The samples were annealed at 573K for 2 minutes in argon. This anneal was performed to relieve surface thermal tempering stresses incurred when the plate was cast, which are known to affect the fatigue behavior of the material [12]. The duration of the anneal was sufficiently small relative to the relaxation time at that temperature (~20 hours at 573K) so the material did not have time to structurally relax during the anneal, as was confirmed previously by Launey *et al*. [12].

### *2.2. Test Environment*

Cyclic fatigue crack growth rate measurements were performed on two stress-relieved C(T) samples in a flowing dry nitrogen atmosphere at roughly 25°C. $N_2$ gas was flowed through a purifier (Gatekeeper, Aeronex, San Diego, CA) rated to achieve sub parts per billion (ppb) levels of oxygen and moisture and into the aluminum and stainless steel test chamber. Before testing, a bake-out procedure was performed to remove contaminants from the test chamber. The tubing and chamber were heated to approximately 140°C while purified $N_2$ flowed through the test setup. After the

chamber reached temperature, it was evacuated to about ~1 Pa using a roughing pump, then backfilled with purified $N_2$ three times to rinse the chamber. After the third rinse, the chamber was left to cool to room temperature for approximately 10 hours while purified $N_2$ continued to circulate through the test setup, after which fatigue testing was conducted. Based on previous investigations [47], it was estimated that the gas entering the chamber contained < 50 ppb of moisture.

*2.3. Fatigue Crack Growth Measurements*

Fatigue testing was performed on a computer controlled servo-hydraulic mechanical testing machine with constant frequency ($v$ = 25 Hz) sine wave loading and a constant ratio of minimum to maximum load ($R = P_{min}/P_{max} = 0.1$). As specified in ASTM E647 [46], the fatigue crack growth rates ($da/dN$) were recorded as a function of applied stress intensity range ($\Delta K = K_{max} - K_{min}$), where $K_{min}$ and $K_{max}$ are the minimum and maximum stress intensity applied to the sample during the loading cycle.

One sample was fatigue cracked with a decreasing stress intensity range using a constant $\Delta K$ gradient ($(d\Delta K/da) \cdot \Delta K^{-1} = -0.08\ mm^{-1}$) until the growth rate approached ~$10^{-10}$ m/cycle in order to measure the slower growth rates and the fatigue threshold, $\Delta K_{TH}$. The other sample was fatigue cracked with a constant load range ($\Delta P$ = 304N) to determine faster fatigue crack growth rates. A strain gage was affixed to the back surface of each sample, and used to monitor crack length progression in the specimen using calibrations for the C(T) geometry [48]. After the crack growth

measurements were performed, the fracture surfaces were analyzed in a scanning electron microscope (SEM).

### 3. Results

A comparison of the fatigue crack growth rates (*da*/*dN*), plotted as a function of applied stress intensity range (Δ*K*), for samples tested in ambient laboratory air and purified dry $N_2$ is shown in Figure 4. Ambient laboratory air data were taken from Ref. [12]. The fatigue crack growth curve obtained in air showed four defined growth rate regimes, detailed in Figure 5a, while the growth curve obtained in purified dry $N_2$ demonstrated only three distinct regimes, shown in Figure 5b.

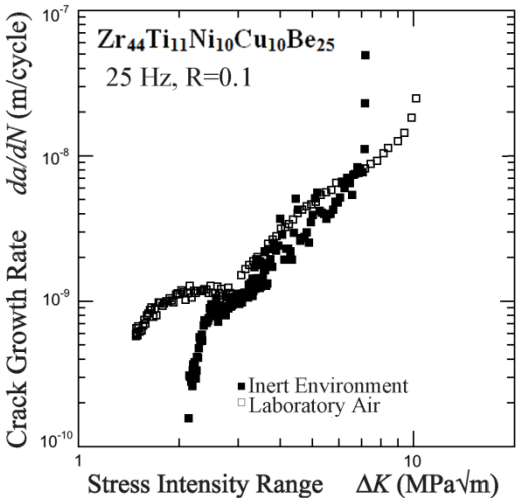


**Figure 4: Fatigue crack growth rates (*da*/*dN*) plotted as a function of applied stress intensity range (Δ*K*), for a $Zr_{44}Ti_{11}Ni_{10}Cu_{10}Be_{25}$ BMG tested in ambient laboratory air and purified dry $N_2$. Air data were taken from Ref. [12].**

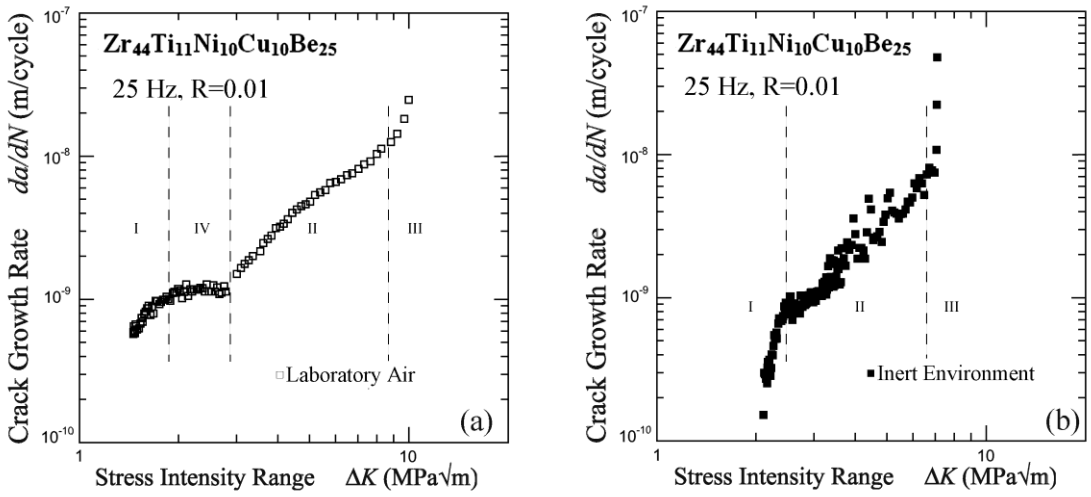


**Figure 5: Fatigue crack growth rate (*da/dN*) plotted as a function of applied stress intensity range (Δ*K*), for $Zr_{44}Ti_{11}Ni_{10}Cu_{10}Be_{25}$. In (a), four discernible growth rate regions are seen for the laboratory air data from Ref. [12], while in (b) three distinguishable growth rate regions are indicated for the purified dry $N_2$ experiments.**

Region I in both cases is a discernable low-growth-rate threshold regime where growth rate is highly sensitive to changes in Δ*K*. Region II is, in each fatigue curve, a distinct intermediate-growth-rate regime in which crack growth rates increase with increasing Δ*K* according to the Paris law. Region III is a high-growth-rate region where $K_{max}$ approaches the fracture toughness of the material and final fracture occurs. Region IV is observed only in the fatigue growth curve obtained in air. It is a regime in which crack growth rate is relatively constant at ~$10^{-9}$ m/cycle and insensitive to changes in Δ*K*.

The medium-growth rates for each fatigue curve (Region II) were analyzed according to the Paris Law using units of m/cycle for *da/dN* and MPa√m for Δ*K* [18]:

$$\frac{da}{dN} = C\Delta K^m \qquad (2)$$

For the data obtained in laboratory air, $C$ was found to equal $1.8 \times 10^{-10}$ MPa$^{-2}$·cycle$^{-1}$ and $m$ was found to be 2.0; $\Delta K_{TH}$ was reported to be <1.5 MPa√m [12]. In the present study, $C$ and $m$ were found to be $8.5 \times 10^{-11}$ MPa$^{-2.3}$·m$^{-0.15}$·cycle$^{-1}$ and ~2.3 respectively for the data obtained in dry $N_2$, and $\Delta K_{TH}$ is ~2.1 MPa√m.

Finally, the fracture surfaces of both samples tested in dry $N_2$ were imaged in an SEM. In general, the features on the fracture surfaces appear to coarsen with increasing $\Delta K$ and fatigue striations are seen at high magnifications, as has been reported for studies conducted in ambient air [12]. Comparing micrographs for samples tested in purified dry $N_2$ with those from previous studies in ambient air revealed that the fatigue surfaces had similar appearances for like growth rates. Example micrographs comparing a fracture surface for a sample from the present study with one from Ref. [12] are shown in Figure 6.

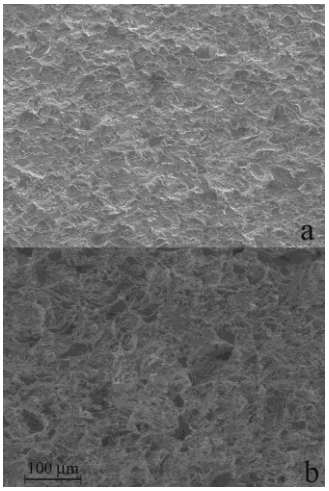


**Figure 6: Scanning electron micrograph comparisons of medium-growth-rate fatigue fracture surfaces: (a) sample fatigued in purified dry $N_2$ (b) sample fatigued in laboratory air. $\Delta K$ was ~ 3 MPa√m for both samples and the nominal crack growth direction was left to right.**

**4. Discussion**

The present $Zr_{44}Ti_{11}Ni_{10}Cu_{10}Be_{25}$ BMG, when tested in dry inert atmosphere, exhibits a significantly higher fatigue threshold, $\Delta K_{TH}$, and a characteristic 3-region fatigue curve, as seen in Figure 4. The plateau in the crack growth curve near ~$10^{-9}$ m/cycle, shown as Region IV in Figure 5(a), is not present in the fatigue curve measured in purified dry $N_2$ indicating that the fatigue behavior is degraded by an ambient air environment. Environmental effects on metallic glasses have been documented in the literature [22, 23, 25, 26, 28, 29, 37-43], and both oxidation and hydrogen embrittlement are identified as possible mechanisms which could affect fatigue crack growth rates in ambient air.

Zr-based metallic glasses are known to form thin, passive protective surface layers resistant to ionic and electrical conductivity [22, 40, 43]. In general, zirconium oxidizes preferentially in Zr-based amorphous metals, often impeding the formation of oxides formed by less reactive elements such as Ni and Cu [22, 23, 37, 39-41, 43]. XPS measurements specifically on Zr-Ti-Cu-Ni-Be based BMGs have shown native oxide films primarily of $ZrO_2$, with small amounts of Be and Ti oxides [43]. Monolayers of oxide can form in nanoseconds at atmospheric pressure; indeed, King, *et. al*. calculate that cyclic fatigue tests performed up to 100Hz can form an oxide monolayer every cycle at room temperature in laboratory air [24]. However, it is noted that the partial pressures of oxygen and water may be much different at a crack tip, so it is difficult to predict the exact frequencies at which surface oxidation may affect fatigue crack growth rates. Moreover, it is often found that testing metals in inert

environments actually increases the near threshold growth rates and lowers the fatigue threshold relative to testing in air due to the mechanism of oxide induced crack closure [24, 49]. In the present study, the higher fatigue threshold in the inert environment indicates that oxide induced crack closure is not a dominant mechanism in this BMG in room air. The latter conclusion is consistent with the absence of short crack fatigue affects in Zr-Ti-Cu-Ni-Be BMGs tested in air [50].

Some traditional hydrogen embrittlement mechanisms for crystalline metals, such as brittle hydride formation or bond decohesion, are also feasible for Zr-based metallic glasses, while additional mechanisms related to the filling of free volume have also been suggested [25, 28, 29]. While the effect of H on the mechanical properties of metallic glasses can vary for different alloys [25], it is generally agreed that H can readily absorb into the free volume of metallic glasses [22, 25, 26], and H has been shown to preferentially sit near Zr atoms in a $Zr_{60}Ti_2Cu_{20}Al_{10}Ni_8$ BMG [51]. For Zr-Ti-Cu-Ni-Be based BMGs, it has been reported that the flow stress increases, and the fracture toughness decreases, with hydrogen charging, indicating a hydrogen embrittlement effect [28, 29]. Furthermore, during fatigue loading of a metallic glass, high levels of plastic deformation increase the amount of free volume in the plastic zone ahead of the crack tip [12, 20, 52]. Thus, H atoms may be able to enter the BMG more easily near the crack tip during fatigue loading.

Interestingly, studies on hydrogen charged $Zr_{41.2}Ti_{13.8}Cu_{12.5}Ni_{10}Be_{22.5}$ have actually shown a decrease in fatigue crack growth rates and an increase in the fatigue threshold with increasing hydrogen charging [28]. This suggests that hydrogen may

retard fatigue crack growth, which was attributed to a combination of i) roughness induced crack closure and ii) the filling of free volume causing a change in the plastic flow behavior. Extensive hydrogen charging caused a very tortuous crack path, causing significant crack closure. However, samples tested in air show a straight crack path in both [28] and [12], similar to the present samples tested in inert atmosphere. Thus, roughness induced crack closure does not seem to be an important mechanism for the present environmental effect. Suh and Dauskardt point out that the overall fatigue crack behavior of hydrogen charged $Zr_{41.2}Ti_{13.8}$ $Cu_{12.5}Ni_{10}Be_{22.5}$ results from a mutual competition of intrinsic embrittling mechanisms and extrinsic shielding mechanisms. Thus, small amounts of hydrogen entering the crack tip, perhaps from oxidation reactions with water vapor, may cause the material to behave drastically different than a BMG that was heavily hydrogen charged. In other words, the balance of this competition may be shifted under different conditions of hydrogen exposure.

Accordingly, while oxide or roughness induced closure don't appear to play a role in the present affects, surface oxidation, hydrogen embrittlement, or a combination of the two may be important factors in causing the observed corrosion fatigue effect in Zr-Ti-Cu-Ni-Be based BMGs. It is also interesting to note that fatigue life experiments on Zr-Al-Cu and Zr-Al-Cu-Ni BMGs have shown no discernable difference in the S/N curves and fatigue limits for samples tested in air and vacuum [53]. While it is difficult to make direct links between the fatigue limit and fatigue threshold since the former is affected by both crack initiation and growth, such observations do indicate that all BMGs may not be expected to have a similar

degrading environmental effect on the fatigue behavior in ambient air. Accordingly, future research will be necessary to determine the exact mechanism(s) involved and how the specific BMG chemistry plays a role.

## 5. Conclusions

Based on a study of the fatigue behavior of a $Zr_{44}Ti_{11}Ni_{10}Cu_{10}Be_{25}$ bulk metallic glass tested in an inert dry $N_2$ environment, it is clear an ambient air environment causes a significant corrosion fatigue effect. When tested in dry $N_2$, $Zr_{44}Ti_{11}Ni_{10}Cu_{10}Be_{25}$ exhibits both a significantly higher $\Delta K_{TH}$ and classical 3-region fatigue curve without the plateau in the crack growth curve near $10^{-9}$ m/cycle observed in other studies conducted in laboratory air.

## Acknowledgements

The authors thank Dr. J. Schroers from Yale University for supplying the material, Dr. M. E. Launey of Lawrence Berkeley National Laboratory for helping heat treat the samples, and Dr. Ralf Busch of Universität des Saarlandes for many useful discussions.

# IV. Manuscript II

## Fracture and Fatigue Behavior of a $Zr_{58.5}Cu_{15.6}Ni_{12.8}Al_{10.3}Nb_{2.8}$ Bulk Metallic Glass Forming Alloy

S. L. Philo[a], H. Lu[b], I. Gallino[b], R. Busch[b], and J. J. Kruzic[a]

[a] Materials Science, School of Mechanical, Industrial, and Manufacturing Engineering, Oregon State University, Corvallis, Oregon, 97331, USA

[b] Universität des Saarlandes, Lehrstuhl für Metallische Werkstoffe 66041 Saarbrücken, Germany

For submission to

*Acta Materialia*

**Abstract**

An initial study into the fracture and fatigue properties of a $Zr_{58.5}Cu_{15.6}Ni_{12.8}Al_{10.3}Nb_{2.8}$ bulk metallic glass was conducted. A fatigue crack growth curve was obtained in ambient air, demonstrating a fatigue threshold of $\Delta K_{TH}$ = 1.4 MPa√m and a Paris law exponent of 1.7. A regime of nearly stress intensity-independent crack growth occurred near a crack growth rate of $2.5 \times 10^{-8}$ m/cycle, suggesting an environmental influence on the fatigue crack growth. The apparent plane strain fracture toughness ($K_C$) was found to average ~26 MPa√m, comparable to values reported for $Zr_{44}Ti_{11}Ni_{10}Cu_{10}Be_{25}$ and $Zr_{41.25}Ti_{13.75}Ni_{10}Cu_{12.5}Be_{22.5}$. However, extensive crack branching caused during $K_C$ testing was observed in each of the measured samples, making the determination of a single value of the fracture toughness questionable.

## 1. Introduction

Bulk metallic glasses (BMGs) are a relatively new class of engineering materials with unique and unusual properties that make them potential candidates for many structural applications [30]. Favorable properties include near theoretical strengths combined with reasonable fracture toughness, low damping, large elastic strain limits, and the ability to be thermoplastically formed into precision shaped parts with complex geometries [31, 32], all of which are generally distinct from, or superior to, corresponding crystalline metals and alloys. The most studied metallic glass forming alloys are of the Zr-Ti-Ni-Cu-Be system, but the presence of beryllium

presents manufacturing problems due to the health hazards posed by handling pure Be metal and its oxidation products. Beryllium-free metallic glass forming alloys are a potential solution to producing Zr-based bulk metallic glasses (BMGs) without the safety risks associated with handling beryllium. $Zr_{58.5}Cu_{15.6}Ni_{12.8}Al_{10.3}Nb_{2.8}$ (Vit 106a)[3] is a promising Be-free metallic glass forming alloy, with a critical cooling rate as low as 1.75 K/s [6, 7]. The purpose of this paper is to provide a first investigation into the fracture and fatigue crack growth behavior of a $Zr_{58.5}Cu_{15.6}Ni_{12.8}Al_{10.3}Nb_{2.8}$ BMG.

## 2. Experimental Methods

### *2.1. Materials*

Fully amorphous $Zr_{58.5}Cu_{15.6}Ni_{12.8}Al_{10.3}Nb_{2.8}$ plates were cast and analyzed using differential scanning calorimetry (DSC), x-ray diffraction (XRD), scanning electron microscopy (SEM), and wavelength dispersive spectroscopy (WDS). Three roughly 3 mm thick cast plates were machined into six compact tension C(T) samples (width, $W$ = 20 mm, thickness, $B$ = 2 mm) in accordance with the standard ASTM E647 [46]. The faces of each sample were subsequently polished to 0.05μm to facilitate accurate crack length measurement.

The samples were annealed at 573K for 2 minutes in argon to relieve surface stresses incurred by thermal tempering during casting, which are known to affect the fatigue behavior of Zr-based BMGs [12]. The duration of the anneal was sufficiently

[3] All compositions are given in terms of atomic percent.

small relative to the relaxation time at that temperature (~28 hours at 573K [6, 7]) so it is assumed that the material did not have time to structurally relax during the anneal, as has been confirmed in other studies [12].

*2.2. Fatigue Crack Growth Measurements*

Fatigue testing was performed using a computer controlled servo-hydraulic mechanical testing machine with constant frequency ($v$ = 25 Hz) sine wave loading and a constant ratio of minimum to maximum load ($R = P_{min}/P_{max} = 0.1$). As specified in ASTM E647 [46], the fatigue crack growth rates ($da/dN$) were recorded as a function of applied stress intensity range ($\Delta K = K_{max} - K_{min}$), where $K_{min}$ and $K_{max}$ are the minimum and maximum stress intensity sustained by the sample during the loading cycle.

To obtain the fatigue growth curve, four samples were used. Three samples were tested under decreasing $\Delta K$ conditions. After pre-cracking at $\Delta K \approx$ 6-8 MPa$\sqrt{m}$, the stress intensity range was then stepped down to an initial value and then slowly decreased using a constant $\Delta K$ gradient ($d\Delta K/da/\Delta K$ = -0.08/mm). Initial values of 5.6, 3.6, and 1.9 MPa$\sqrt{m}$ were used, allowing the measurement of a wide range of mid to low growth rates, and the fatigue threshold, $\Delta K_{TH}$, which was defined as the $\Delta K$ for which the growth rate approached ~$10^{-10}$ m/cycle. For each decreasing $\Delta K$ test, data collection began after the crack had progressed outside of the calculated plane strain plastic zone formed at $K_{max}$ during pre-cracking to avoid transient effects. The fourth sample was fatigue cracked with a constant load range ($\Delta P$ = 194N) beginning at $\Delta K$

≈ 6 MPa√m to determine higher fatigue growth rates. A strain gage was affixed to the back surface of each sample, and used to monitor crack length progression in the specimen with calculations performed using standard calibrations for the C(T) geometry [48].

*2.3. Fracture Testing*

After the crack growth measurements were performed, plane strain fracture toughness was determined using the remaining material from the three decreasing $\Delta K$ tests by monotonically loading with a displacement rate of 20 μm/s. The apparent fracture toughness, $K_c$, was calculated based on the peak load at fracture. Based on indications of crack branching behavior during such testing, one of the three tests was interrupted just after the peak load was achieved, but prior to final fracture, to observe the crack branches. After those observations were made, the sample was re-loaded at a 20 μm/s displacement rate and the branches were extended but again testing was interrupted before final fracture. Finally, the sample was loaded at a 20 μm/s displacement rate until final fracture occured. The fracture surfaces and crack profiles were observed in optical and scanning electron microscopes (OM and SEM).

**3. Results**

*3.1. Material*

The bulk of the plates were confirmed to be fully amorphous by both DSC and XRD (Figure 7). Backscatter SEM imaging revealed the presence of crystalline inclusions and WDS results indicated those inclusions to contain approximately 1%

Fe, a contaminant likely from the stainless steel molds. Indeed, inclusions were highly concentrated near the mold walls, where XRD analysis was sensitive enough to confirm their crystalline nature and reveal that the inclusions were not all of the same crystal structure. However, after machining away ~0.5 mm of the mold interface layer from each side, the remaining inclusions were generally dispersed in the fully amorphous matrix and undetectable by XRD (Fig. 7).

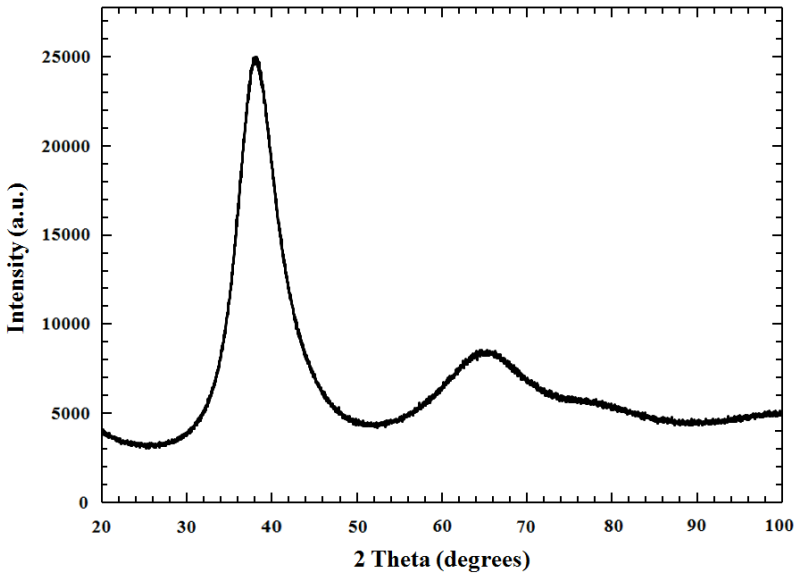


**Figure 7: X-ray diffraction (XRD) scan of fully amorphous $Zr_{58.5}Cu_{15.6}Ni_{12.8}Al_{10.3}Nb_{2.8}$. The scan was run at 0.1 degrees per second at room temperature.**

*3.2 Fatigue Crack Growth*

Fatigue crack growth rates ($da/dN$), plotted as a function of applied stress intensity range ($\Delta K$), for Vit 106a are shown in Figure 8. For comparison to a Be containing BMG, data for a $Zr_{44}Ti_{11}Ni_{10}Cu_{10}Be_{25}$ BMG (Vit 1b) taken from Ref. [12] are shown as well. Each of the fatigue crack growth curves, obtained in ambient laboratory air, showed four distinct regimes, detailed in Figure 9a and Figure 9b.

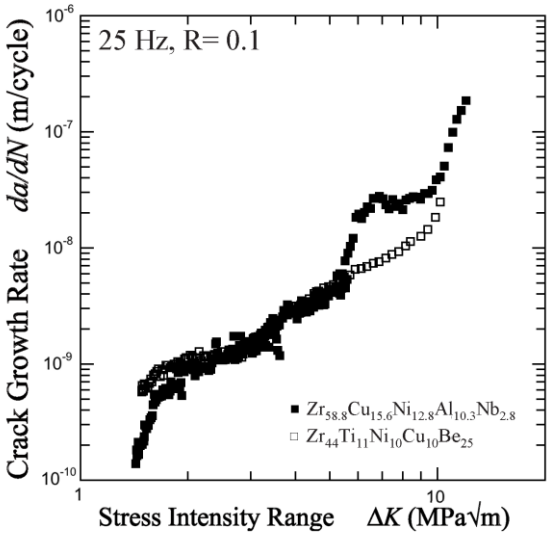


**Figure 8: Fatigue crack growth rates (*da*/*dN*) plotted as a function of applied stress intensity range (Δ*K*), for $Zr_{44}Ti_{11}Ni_{10}Cu_{10}Be_{25}$ and $Zr_{58.5}Cu_{15.6}Ni_{12.8}Al_{10.3}Nb_{2.8}$ BMGs tested in laboratory air. Data for $Zr_{44}Ti_{11}Ni_{10}Cu_{10}Be_{25}$ were taken from Ref. [12].**

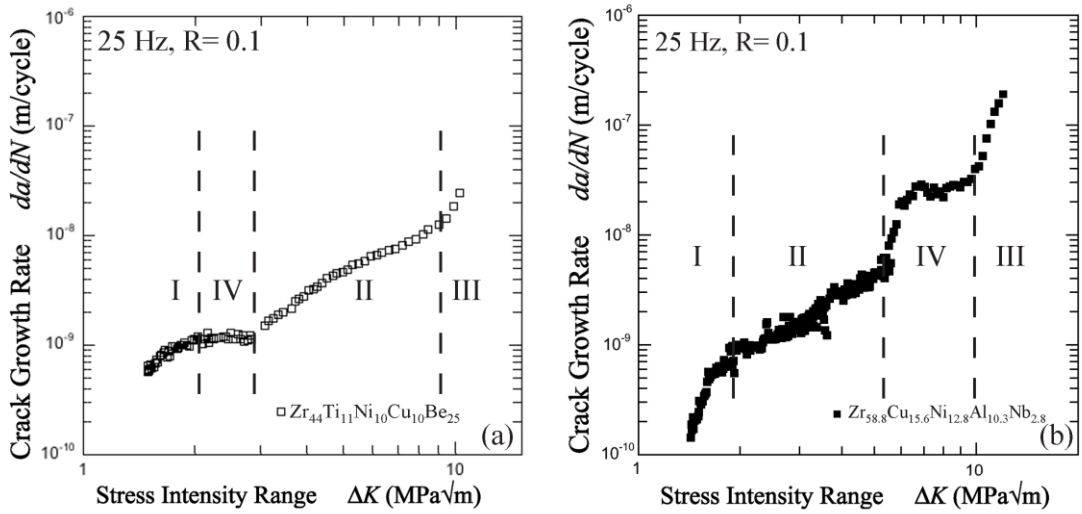


**Figure 9: Fatigue crack growth rate (*da/dN*) plotted as a function of applied stress intensity range (Δ*K*), in laboratory air. In (a), four discernible growth rate regions are seen for $Zr_{44}Ti_{11}Ni_{10}Cu_{10}Be_{25}$ data from Ref. [12] with a plateau at ~$10^{-9}$ m/cycle, while in (b) $Zr_{58.5}Cu_{15.6}Ni_{12.8}Al_{10.3}Nb_{2.8}$ shows a plateau at ~$2.5 \times 10^{-8}$ m/cycle.**

Region I in both cases is a discernable low-growth-rate threshold regime where the growth rate is highly sensitive to changes in $\Delta K$. Region II is, in each fatigue curve, a distinct intermediate-growth-rate regime in which crack growth increases with increasing $\Delta K$ according to the Paris law. Region III is a high-growth-rate region where $K_{max}$ approaches the fracture toughness of the material and final fracture occurs. Region IV is a regime in which crack growth rate is relatively insensitive to changes in $\Delta K$, found near $10^{-9}$ m/cycle for Vit 1b, and near $2.5 \times 10^{-8}$ m/cycle for Vit 106a.

The medium-growth rates for each fatigue curve (Region II) were fit to the classical Paris Law using units of m/cycle for *da/dN* and MPa√m for $\Delta K$ [18]:

$$\frac{da}{dN} = C\Delta K^m \qquad (2)$$

For the Vit 1b data, $C$ was found to equal $1.8 \times 10^{-10}$ $MPa^{-2}\cdot cycle^{-1}$ and $m$ was found to be 2.0; $\Delta K_{TH}$ is shown to be < 1.5 MPa√m. $C$ and $m$ were found to be $3 \times 10^{-10}$ $m^{0.15}\cdot MPa^{-1.7}\cdot cycle^{-1}$ and ~1.7 respectively for Vit 106a, and $\Delta K_{TH}$ is 1.4 MPa√m.

### *3.3. Fracture*

The mean $K_c$ value for the three tests was found to be approximately 26 MPa√m based on the individual values shown in Table 2. For the test which was interrupted, branching was observed at the crack tip using OM, as shown in Figure 10a, and the value in Table 2 is calculated based on the peak load during the first loading of the sample. Loading was then re-applied to a higher level (Table 3) and again the test was stopped for observation. The crack tip was examined a second time and the branches

were found to have elongated (Figure 10b). The sample was then loaded until final fracture occurred. With each loading sequence there was an increase in the apparent toughness, as detailed in Table 3. Finally, post fracture examination of samples that were simply loaded to fracture revealed branching occurred in each sample (Figure 10c).

**Table 2: Plane strain fracture toughness data**

| Sample | Plane Strain Fracture Toughness, $K_C$ |
|---|---|
| **1** | 15.8 MPa√m |
| **2** | 28.9 MPa√m |
| **3** | 32.1* MPa√m |

*Loading of Sample 3 was stopped immediately after a slight drop in load was observed. Calculated $K_c$ value is based on that initial peak value, although higher loads were achieved upon re-loading.

**Table 3: Loading sequence for Sample 3**

| | Maximum or peak load | Apparent toughness, $K_C$* |
|---|---|---|
| **Initial loading** | 636 N | 32.1 MPa√m |
| **2nd loading** | 1000 N | 50.5 MPa√m |
| **Final loading** | 1944 N | 98.2 MPa√m |

*Apparent toughness was calculated based on the initial fatigue crack length (before branching) and the maximum or peak load achieved during each loading run.

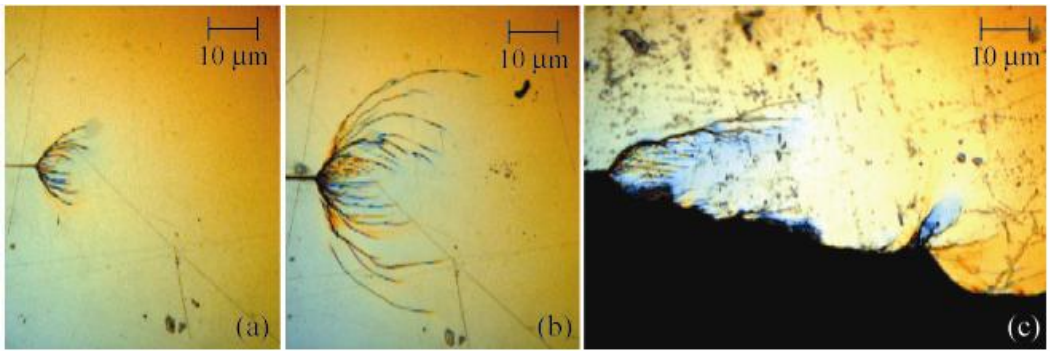


**Figure 10: Optical micrograph comparisons of crack branching perpendicular to the initial crack plane: (a) after initial $K_c$ test interruption for Sample 3 (b) branch growth after Sample 3 was re-loaded to higher level (c) scalloped edge evidences crack branching in broken Sample 1.**

*3.4. Fractography*

The fracture surfaces of each Vit 106a sample were imaged in a scanning electron microscope (SEM) (Figs. 11). In general, the features on the fracture surfaces appear to coarsen with increasing $\Delta K$ (Figure 12), as has been reported for a $Zr_{44}Ti_{11}Ni_{10}Cu_{10}Be_{25}$ BMG [12].

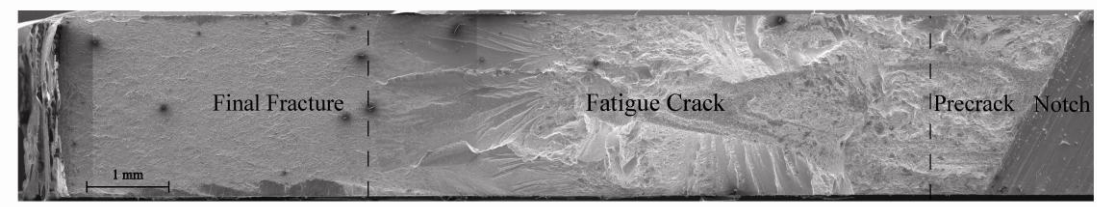


**Figure 11: Scanning electron micrograph of $Zr_{58.5}Cu_{15.6}Ni_{12.8}Al_{10.3}Nb_{2.8}$ fracture surface, with crack propagating from the right hand side of the image toward the left hand side of the image. This micrograph of Sample 1 shows the rough surface morphology found in each sample.**

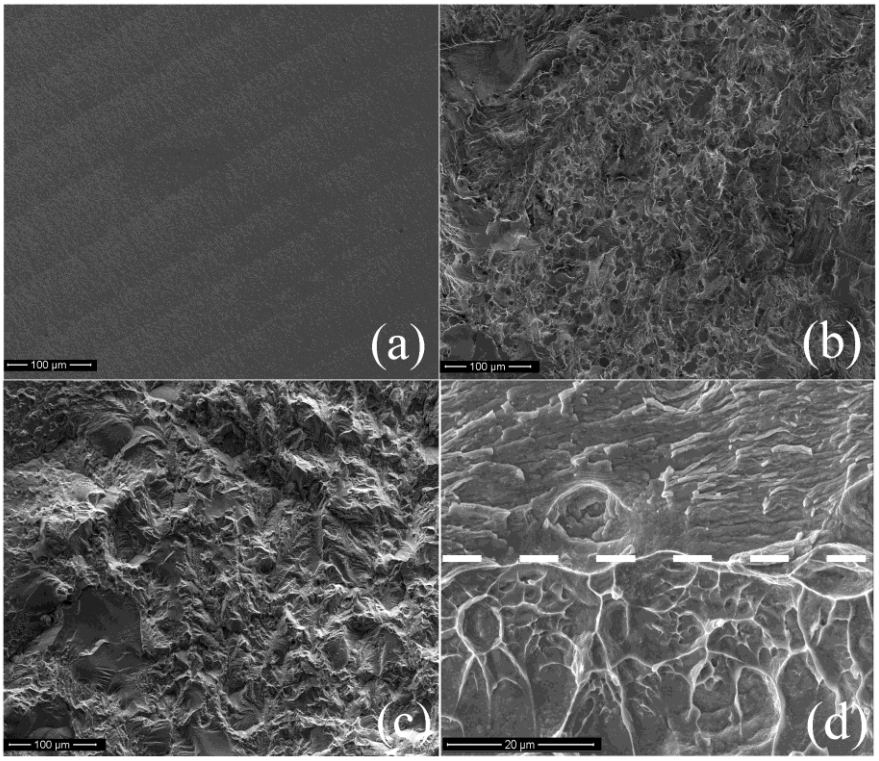


**Figure 12: Scanning electron micrographs of $Zr_{58.5}Cu_{15.6}Ni_{12.8}Al_{10.3}Nb_{2.8}$ fracture surfaces, with crack propagating from the top of the image toward the bottom of the image: (a) low stress intensity ($\Delta K \sim 3$), (b) medium stress intensity ($\Delta K \sim 6$), (c) high stress intensity ($\Delta K \sim 10$), (d) fatigue striations on the top of the micrograph growing into vein-like morphology on the bottom of the micrograph, approximately indicated by the dashed line, as final fracture occurred ($\Delta K \sim 15$).**

## 4. Discussion

### *4.1 Environmental Effect*

Vit 106a tested in ambient room air exhibits a similar fatigue curve, including fatigue threshold ($\Delta K_{TH}$) and $K_{max}$, to that of Vit 1b under similar experimental conditions. However, while both materials exhibit plateaus in the crack growth curve, they occur at different crack growth rates; near $10^{-9}$ m/cycle for Vit 1b, and at approximately $2.5 \times 10^{-8}$ m/cycle for Vit 106a, shown as Region IV in Figs. 9(a) and

9(b), respectively. It is also interesting to note that a $Zr_{41.25}Ti_{13.75}Ni_{10}Cu_{12.5}Be_{22.5}$ (Vit 1) also has shown a similar plateau at $10^{-9}$ m/cycle [11], suggesting similar behavior occurs for the various Zr-Ti-Ni-Cu-Be based BMGs. In the fatigue of materials, such behavior generally indicates something other than mechanical loading acts as the rate limiting step in the crack growth process, and that commonly is an interaction with the environment [44, 45]. Indeed, a recent study has shown for Vit 1b that the plateau does not occur for samples tested in purified $N_2$ gas [54]. While it is currently unclear what exact mechanism is responsible for this corrosion fatigue effect, both crack tip oxidation and hydrogen embrittlement and have been considered as possibilities [54]. From the present data, however, it is clear that the rate limiting step of the environmental effect is faster for Vit 106a than for Vit 1b since it is seen at higher growth rates.

The growth rate associated with the plateau is often associated with the critical rate for the aggressive species to either diffuse to the crack tip, or to diffuse into the material ahead of the crack tip. In either case, the diffusivity in Vit 106a would appear to be higher, since the plateau occurs at a higher growth rate. Alternatively, the difference in the plateau locations between Vit 1b and Vit 106a may also relate, in part, to the fact that Be-free metallic glasses tend to be more susceptible to oxide formation than Be-containing alloys [11]. For example, a thicker oxide along the crack wake may provide some protection of the crack tip at lower stress intensities, while higher stress intensities may open the crack sufficiently for the species to reach the crack tip. Ultimately, a better understanding of environmental effects on the fatigue

properties of BMG's is needed in order to fully explain differences among alloys; however, it is clear that altering alloy chemistry may be a way to tailor BMGs to avoid detrimental environmental effects. Indeed, there is a pronounced difference in behavior between $Zr_{58.5}Cu_{15.6}Ni_{12.8}Al_{10.3}Nb_{2.8}$ and Zr-Ti-Ni-Cu-Be based BMGs.

*4.2 Crack Branching*

Vit 106a demonstrated crack branching during plane-strain fracture toughness ($K_c$) determination, as shown in Fig. 4, which can lead to very high apparent toughness (Table 2). Similar crack branching and high apparent toughness has been observed by Flores and Dauskardt in the fracture of a $Zr_{41.25}Ti_{13.75}Ni_{10}Cu_{12.5}Be_{22.5}$ BMG (Vit 1) tested using single edge notched samples loaded in tension, SEN(T) [55]. For the SEN(T) geometry, they argued that such behavior was promoted because the slip lines ahead of the crack tip form at 45° to the loading axis, allowing shear bands to diverge from the main crack tip. Conversely, if the driving force for crack branching was purely related to the slip line fields, such behavior should not be promoted by C(T) or SEN(B) geometries [55]. That is because the bending component of the loading causes Prandtl slip fields which should cause slip bands in the BMG to bend back to the crack plane. Thus, while the SEN(T) geometry may help promote such behavior, the observation of crack branching in C(T) samples in the present study suggests that crack branching in BMGs cannot simply be explained for all cases by slip line fields and there is some other fundamental mechanism involved in the present case.

As previously mentioned, the Vit 106a samples contained crystalline inclusions dispersed throughout a fully amorphous matrix. Their presence may promote the formation of crack branches, providing multiple spots for shear band formation to occur. Indeed, it has been suggested that one key to creating high toughness BMG based materials is to have a second phase to prevent single shear band failures [56]. However, no matter the exact cause, crack tip blunting and branching makes true fracture toughness determination difficult. The calculation of a true plane strain fracture toughness according to ASTM standard E399 [57] assumes a single crack propagates across the sample to cause catastrophic failure at a single value of stress intensity. From the present data (Table 2), it is clear samples that are progressively loaded within the crack branch propagation regime can exhibit much higher apparent toughness than those monotonically loaded to failure, causing an apparent rising fracture resistance with crack extension, or rising *R*-curve effect. Such behavior is not only loading rate sensitive, which is well documented for the toughness of Zr-based BMGs [11, 12], but also history dependent, since drastically higher apparent toughness was obtained for Sample 3 where testing was interrupted and reloading was conducted.

Because evidence of crack branching was seen in all samples in the present study, a single fracture toughness value may prove elusive. While the highest apparent toughness values observed here are likely non-conservative from a design standpoint, this BMG shows considerable damage tolerance when crack branching occurs. However, from a design standpoint, it is expected that the lowest measured toughness

values would be used in order to be conservative in avoiding unexpected failures. Considering the strain rate sensitivity of the fracture toughness for BMGs, the highest strain rates give the lowest toughness and are likely be the most relevant. In the present study, based on Fig. 2 the fatigue sample grown at constant stress range reached fatigue instability at $K_{max}$ = 17.6 MPa√m. This is similar to the lowest value of 15.8 MPa√m in Table 2 found for the fracture tests, and also similar to fatigue instability values reported for Vit 1 [11] and Vit 1b [12].

Flores and Dauskardt analyzed parallel branched cracks growing in Vit 1 for the SEN(T) geometry and found that while the apparent toughness rose as high as 134 MPa√m in one case, the individual cracks experienced much lower stress intensity, on the order of 15 MPa√m [55]. Similar stress intensity solutions are not available for parallel cracks in the C(T) loading configuration; however, it is assumed that the individual crack tips in Vit 106a likely experience similar stress intensities as found in [55] for Vit 1 considering the fatigue instability value, and the lowest fracture value, are of similar magnitude. Thus, in general the fracture toughness of Vit 106a appears in line with BMGs of the Zr-Ti-Ni-Cu-Be system.

## 5. Conclusion

Based on a first study of the fracture and fatigue behavior of a $Zr_{58.5}Cu_{15.6}Ni_{12.8}Al_{10.3}Nb_{2.8}$ bulk metallic glass (Vit 106a), the following conclusions are made:

1. Fatigue crack growth behavior was found to be similar to Zr-Ti-Ni-Cu-Be BMGs, with a fatigue threshold of $\Delta K_{TH}$ = 1.4 MPa√m, a Paris law exponent of 1.7, and a regime where crack growth was roughly independent of the applied stress intensity, suggesting a strong influence of the ambient environment. However, a key difference between the fatigue crack growth behavior of $Zr_{58.5}Cu_{15.6}Ni_{12.8}Al_{10.3}Nb_{2.8}$ and Zr-Ti-Ni-Cu-Be BMGs is the growth rate where that plateau occurs, $10^{-9}$ and $2.5 \times 10^{-8}$ m/cycle respectively. Such results indicate altering alloy chemistry may be a way to mitigate such environmental degradation of the fatigue properties by ambient air.

2. The apparent plane strain fracture toughness ($K_C$) was found to average ~26 MPa√m, comparable to values reported for Zr-Ti-Ni-Cu-Be BMGs. However, crack branching, previously never observed in BMGs for the C(T) sample geometry, was seen in each of the measured samples during $K_C$ testing, making the determination of a single value of the fracture toughness questionable. Such crack branching may be

related to the presence of inclusions, which can provide initiation sites for multiple shear bands.

3. For conservative design practices, it is likely the lowest attainable fracture toughness values will need to be used in order to avoid unwanted failures. In that regard, the stress intensity where fatigue instability occurs may the most conservative assessment. In the present study, a value of ~17 MPa√m was found for Vit 106a, which again is similar to those reported for Zr-Ti-Ni-Cu-Be BMGs.

**Acknowledgements**

# V. Summary and Conclusion

The influence of aggressive environment on the fatigue properties of two metallic glasses, $Zr_{44}Ti_{11}Ni_{10}Cu_{10}Be_{25}$ and $Zr_{58.5}Cu_{15.6}Ni_{12.8}Al_{10.3}Nb_{2.8}$ was considered in this study. $Zr_{44}Ti_{11}Ni_{10}Cu_{10}Be_{25}$ was proven to be susceptible to environmental aggression when fatigue tested in an ambient air environment. Neither hydrogen embrittlement nor oxide wedging mechanisms fit the obtained data. More research needs to be done both to isolate the aggressive species, and to determine the aggression mechanism for Zr-based metallic glasses.

$Zr_{58.5}Cu_{15.6}Ni_{12.8}Al_{10.3}Nb_{2.8}$ was shown to produce a similar fatigue curve to $Zr_{44}Ti_{11}Ni_{10}Cu_{10}Be_{25}$, including comparable fatigue threshold and maximum stress values when tested in ambient air, approximately 1.6 MPa√m and10 MPa√m respectively. The only significant difference between the two fatigue curves is the location of the plateau, which is characteristic of an environmental effect and is distinguished by the insensitivity of the crack growth rate to stress intensity. In $Zr_{58.5}Cu_{15.6}Ni_{12.8}Al_{10.3}Nb_{2.8}$ the plateau occurs at a significantly higher crack growth rate ($2.5 \times 10^{-8}$ m/cycle) than it does in $Zr_{44}Ti_{11}Ni_{10}Cu_{10}Be_{25}$ ($10^{-9}$ m/cycle). It is postulated that, should the aggressive species be the same in both materials, the diffusivity of the environmental aggressor would be higher in $Zr_{58.5}Cu_{15.6}Ni_{12.8}Al_{10.3}Nb_{2.8}$. However, no evidence has been provided to establish similarity between the mechanisms influencing the fatigue curves of the two metallic glasses. The differences between the environmental effects found in both materials

could just as easily be explained using differences in aggressive species: it can be argued that $Zr_{58.5}Cu_{15.6}Ni_{12.8}Al_{10.3}Nb_{2.8}$ is more susceptible to oxide formation mechanisms because it lacks beryllium.

The fracture toughness ($K_C$) of Vit 106a was also measured. The determined fracture toughness was comparable to that of other Zr-based metallic glasses; however, crack branching was shown to have occurred during all $K_C$ measurements. Because crack branching does not typically occur during bending, it is unclear whether it occurred because of the crystalline inclusions found in the testing material, or whether it is further evidence of environmental effect. Further testing needs to be done to concretely prove the susceptibility of Vit 106a to environmental aggression, and to determine the cause for crack branching during monotonic loading.

In conclusion, until the exact mechanisms for environmental aggression are understood, it will be difficult to fully predict the effects of environment on the fatigue properties of metallic glasses.

## References

[1] Klement W, Willens RH, Duwez P. Non-crystalline Structure in Solidified Gold–Silicon Alloys. Nature 1960:869.

[2] Inoue A, Kita K, Zhang T, Masumoto T. Materials Transactions, JIM 1989;30:722.

[3] Faupel F, Frank W, Macht MP, Mehrer H, Naundorf V, Ratzke K, Schober HR, Sharma SK, Teichler H. Diffusion in metallic glasses and supercooled melts. Reviews of Modern Physics 2003;75:237.

[4] Greer AL, Ma E. Bulk metallic glasses: At the cutting edge of metals research. Mrs Bulletin 2007;32:611.

[5] Launey ME, Busch R, Kruzic JJ. Influence of structural relaxation on the fatigue behavior of a $Zr_{41.25}Ti_{13.75}Ni_{10}Cu_{12.5}Be_{22.5}$ bulk amorphous alloy. Scripta Materialia 2006;54:483.

[6] Gallino I, Shah MB, Busch R. Enthalpy relaxation and its relation to the thermodynamics and crystallization of the Zr58.5Cu15.6Ni12.8Al10.3Nb2.8 bulk metallic glass-forming alloy. Acta Materialia 2007;55:1367.

[7] Gallino I, Shah MB, Busch R. Enthalpy relaxation of the $Zr_{58.5}Cu_{15.6}Ni_{12.8}Al_{10.3}Nb_{2.8}$ bulk metallic glass forming alloy. Journal of Alloys and Compounds 2007;434:141.

[8] Wright WJ, Hufnagel TC, Nix WD. Free volume coalescence and void formation in shear bands in metallic glass. Journal of Applied Physics 2003;93:1432.

[9] Yavari AR, Lewandowski JJ, Eckert J. Mechanical properties of bulk metallic glasses. Mrs Bulletin 2007;32:635.

[10] Schroeder V, Ritchie RO. Stress-corrosion fatigue-crack growth in a Zr-based bulk amorphous metal. Acta Materialia 2006;54:1785.

[11] Gilbert CJ, Schroeder V, Ritchie RO. Mechanisms for fracture and fatigue-crack propagation in a bulk metallic glass. Metallurgical and Materials Transactions a-Physical Metallurgy and Materials Science 1999;30:1739.

[12] Launey ME, Busch R, Kruzic JJ. Effect of free volume changes and residual stresses on the fatigue and fracture behavior of a Zr-Ti-Ni-Cu-Be bulk metallic glass. Acta Mater. 2008;56:500.

[13] Argon AS. Mechanisms of inelastic deformation in metallic glasses. Journal of Physics and Chemistry of Solids 1982;43:945.

[14] Argon AS. Plastic-deformation in metallic glasses. Acta Metallurgica 1979;27:47.

[15] Schuh CA, Lund AC. Atomistic basis for the plastic yield criterion of metallic glass. Nature Materials 2003;2:449.

[16] Spaepen F. Homogeneous flow of metallic glasses: A free volume perspective. Scripta Materialia 2006;54:363.

[17] Anderson TL. Fracture Mechanics: Fundamentals and Applications. Boca Raton: CRC Press, 2005.

[18] Paris P, Gomez M, Anderson W. A rational analytic theory of fatigue. The Trend in Engineering 1961;13.

[19] Gangloff R. Corrosion Fatigue Crack Propagation in Metals. In: NASA, editor, 1990.

[20] Liu M, Vallery RS, Gidley DW, Launey ME, Kruzic JJ. Assessment of the fatigue transformation zone in bulk metallic glasses using positron annihilation spectroscopy. J. Appl. Phys. 2009;105:093501.

[21] Jiang WH, Jiang F, Green BA, Liu FX, Liaw PK, Choo H, Qiu KQ. Electrochemical corrosion behavior of a Zr-based bulk-metallic glass. Applied Physics Letters 2007;91.

[22] Scully JR, Gebert A, Payer JH. Corrosion and related mechanical properties of bulk metallic glasses. Journal of Materials Research 2007;22:302.

[23] Cocke DL, Liang G, Owens M, Halverson DE, Naugle DG. The oxidation behavior of amorphous and polycrystalline Zr-Ni alloys. Materials Science and Engineering 1988;99:497.

[24] King JE, Cotterill PJ. Role of oxides in fatigue crack-propagation. Materials Science and Technology 1990;6:19.

[25] Eliaz N, Eliezer D. An overview of hydrogen interaction with amorphous alloys. Advanced Performance Materials 1999;6:5.

[26] Libowitz GG, Maeland AJ. Interactions of hydrogen with metallic-glass alloys. Journal of the Less-Common Metals 1984;101:131.

[27] Parkins RN. Environment sensitive fracture of metals. Canadian Metallurgical Quarterly 1992;31:79.

[28] Suh D, Dauskardt RH. Hydrogen effects on the mechanical and fracture behavior of a Zr-Ti-Ni-Cu-Be bulk metallic glass Scr. Mater. 2000;42:233.

[29] Suh D, Dauskardt RH. The effects of hydrogen on deformation and fracture of a Zr-Ti-Ni-Cu-Be bulk metallic glass. Mater. Sci. Eng. A 2001;A319-321:480.

[30] Byrne CJ, Eldrup M. Materials science - Bulk metallic glasses. Science 2008;321:502.

[31] Ashby MF, Greer AL. Metallic glasses as structural materials. Scripta Mater. 2006;54:321.

[32] Schroers J. The superplastic forming of bulk metallic glasses. JOM 2005;57:35.

[33] Launey ME, Hofmann DC, Johnson WL, Ritchie RO. Solution to the problem of the poor cyclic fatigue resistance of bulk metallic glasses. Proc. Natl. Acad. Sci. U. S. A. 2009;106:4986.

[34] Gilbert CJ, Lippmann JM, Ritchie RO. Fatigue of a Zr-Ti-Cu-Ni-Be bulk amorphous metal: Stress/life and crack growth behavior. Scr. Mater. 1998;38:537.

[35] Wang GY, Liaw PK, Peker A, Yang B, Benson ML, Yuan W, Peter WH, Huang L, Freels M, Buchanan RA, Liu CT, Brooks CR. Fatigue behavior of Zr-Ti-Ni-Cu-Be bulk-metallic glasses. Intermetallics 2005;13:429.

[36] Menzel BC, Dauskardt RH. The fatigue endurance limit of a Zr-based bulk metallic glass. Scripta Mater. 2006;55:601.

[37] Liu L, Qiu CL, Chen Q, Chan KC, Zhang SM. Deformation behavior, corrosion resistance, and cytotoxicity of Ni-free Zr-based bulk metallic glasses. Journal of Biomedical Materials Research Part A 2008;86A:160.

[38] Morrison ML, Buchanan RA, Liaw PK, Green BA, Wang GY, Liu CT, Horton JA. Corrosion-fatigue studies of the Zr-based Vitreloy 105 bulk metallic glass. Materials Science and Engineering a-Structural Materials Properties Microstructure and Processing 2007;467:198.

[39] Walz B, Oelhafen P, Guntherodt HJ, Baiker A. Surface oxidation of amorphous Ni-Zr alloys. Applied Surface Science 1989;37:337.

[40] Kimura HM, Asami K, Inoue A, Masumoto T. The oxidation of amorphous Zr-base binary alloys in air. Corr. Sci. 1993;35:909.

[41] Köster U, Jastrow L. Oxidation of Zr-based metallic glasses and nanocrystalline alloys. Mater. Sci. Eng. A 2007;449:57.

[42] Liu CT, Heatherly L, Easton DS, Carmichael CA, Schneibel JH, Chen CH, Wright JL, Yoo MH, Horton JA, Inoue A. Test environments and mechanical properties of Zr-base bulk amorphous alloys. Metall. Mater. Trans. A 1998;29:1811.

[43] Sharma SK, Strunskus T, Ladebusch H, Faupel F. Surface oxidation of amorphous $Zr_{65}Cu_{17.5}Ni_{10}Al_{7.5}$ and $Zr_{46.75}Ti_{8.25}Cu_{7.5}Ni_{10}Be_{27.5}$. Mater. Sci. Eng. A 2001;304:747.

[44] McEvily AJaRPW. Fracture mechanics and corrosion fatigue. *Corrosion Fatigue: Chemistry, Mechanics and Microstructure* 1972.

[45] Suresh S. Fatigue of Materials. Cambridge: Cambridge University Press, 1998.

[46] ASTM E647-00. Annual Book of ASTM Standards, Vol. 03.01: Metals-Mechanical Testing; Elevated and Low-temperature Tests; Metallography. ASTM International, West Conshohocken, Pennsylvania, USA, 2004. p.595.

[47] Kruzic JJ, Cannon RM, Ritchie RO. Effects of moisture on grain-boundary strength, fracture and fatigue properties of alumina. J. Am. Ceram. Soc. 2005;88:2236.

[48] Maxwell DC. Strain based compliance method for determining crack length for a C(T) specimen. Air Force Wright Aeronautical Laboratories, 1987.

[49] Ritchie RO. Mechanisms of fatigue crack propagation in metals, ceramics and composites: role of crack tip shielding. Mater. Sci. Eng. 1988;A103:15.

[50] Menzel BC, Dauskardt RH. Stress-life fatigue behavior of a Zr-based bulk metallic glass. Acta Mater. 2006;54:935.

[51] Mattern N, Gebert A. Hydrogenation of $Zr_{60}Ti_2Cu_{20}Al_{10}Ni_8$ bulk metallic glass. Appl. Phys. Lett. 2003;83:1134.

[52] Vallery RS, Liu M, Gidley DW, Launey ME, Kruzic JJ. Characterization of fatigue induced free volume changes in a bulk metallic glass using positron annihilation spectroscopy. Appl. Phys. Lett. 2007;91:261908.

[53] Wang GY, Liaw PK, Peter WH, Yang B, Yokoyama Y, Benson ML, Green BA, Kirkham MJ, White SA, Saleh TA, McDaniels RL, Steward RV, Buchanan RA, Liu CT, Brooks CR. Fatigue behavior of bulk-metallic glasses. Intermetallics 2004;12:885.

[54] Philo SL, Kruzic JJ. Fatigue crack growth behavior of a Zr-Ti-Cu-Ni-Be bulk metallic glass: Role of ambient air environment. Scr. Mater. 2009:in review.

[55] Flores KM, Dauskardt RH. Enhanced toughness due to stable crack tip damage zones in bulk metallic glass. Scripta Materialia 1999;41:937.

[56] Launey ME, Hofmann DC, Suh JY, Kozachkov H, Johnson WL, Ritchie RO. Fracture toughness and crack-resistance curve behavior in metallic glass-matrix composites. Appl. Phys. Lett. 2009;94:3.

[57] ASTM E399-90 (Reapproved 1997). Annual Book of ASTM Standards, Vol. 03.01: Metals- Mechanical Testing; Elevated and Low-temperature Tests; Metallography. ASTM International, West Conshohocken, Pennsylvania, USA, 2004.